Mucoadhesive and mucopenetrating chitosan nanoparticles for glycopeptide antibiotic administration

Graphical Abstract (for review)

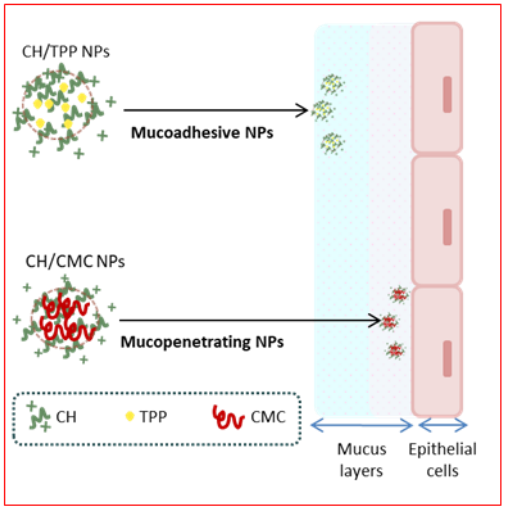

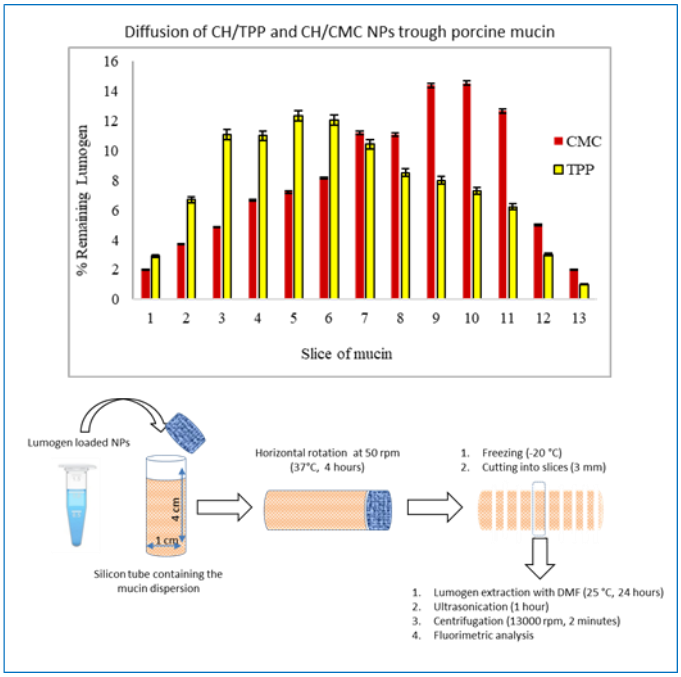

Mucoadhesive and mucopenetrating chitosan nanoparticles for glycopeptide antibiotic administration

Abruzzo A.[1]*, Giordani B.[1], Miti A.[2], Vitali B.[1], Zuccheri G. [2,3], Cerchiara T.[1], Luppi B.[1], Bigucci F.[1]

[1] Department of Pharmacy and Biotechnology, Via San Donato 19/2, University of Bologna, 40127 Bologna, Italy; E-Mails: angela.abruzzo2@unibo.it; barbara.giordani4@unibo.it; b.vitali@unibo.it teresa.cerchiara2@unibo.it; barbara.luppi@unibo.it; federica.bigucci@unibo.it.

[2] Department of Pharmacy and Biotechnology and Interdepartmental Center for Industrial Research on Health Science and Technologies, Via Irnerio 48, Bologna, University of Bologna, 40126 Bologna, Italy; Email: andrea.miti@unibo.it; giampaolo.zuccheri@unibo.it.

[3] S3 Center of the Nanoscience Institute of the Italian Research Council (CNRNANO), Via Campi, 213/A, 41125 Modena, Italy.

* Author to whom correspondence should be addressed: Angela Abruzzo, Department of Pharmacy and Biotechnology, Via San Donato 19/2, University of Bologna, 40127 Bologna, Italy. Tel: +390512095615. E-mail: angela.abruzzo2@unibo.it

Abstract

The use of nanoparticles (NPs) represents a useful strategy for peptide antibiotic delivery to mucosal membranes by either prolonging drug residence time at the target site (mucoadhesive NPs) or by enhancing diffusion across mucus layer to reach the underlying epithelium (mucopenetrating NPs). The purpose of this study was to design chitosan (CH) NPs and to evaluate their employment as mucoadhesive and/or mucopenetrating systems for vancomycin (VM) delivery. NPs were prepared by ionic gelation of CH with sodium carboxymethylcellulose (CMC), sodium alginate (ALG), sodium tripolyphosphate (TPP) or phytic acid (PA) and characterized in terms of size, zeta-potential, morphology, drug encapsulation efficiency, mucoadhesion and mucopenetrating ability. Moreover, *in vitro* tests were conducted to evaluate VM release and the antibacterial activity against *Staphylococcus aureus* and *Bacillus subtilis*. NPs showed sizes ranged from 150 nm to 350 nm with good polydispersity index and positive zeta-potential. The selection of the suitable crosslinker allowed to modulate the mucoadhesive/mucopenetrating properties: CH/TPP NPs showed the best mucoadhesive ability, while CH/PA and CH/CMC NPs were characterized by an improved diffusion across the mucus layer. Further, NPs allowed a fast and complete release of VM, maintaining the antibacterial activity against the tested bacteria species.

Keywords: chitosan nanoparticles, mucoadhesion, mucopenetration, vancomycin, antibacterial activity.

Introduction

Mucosal membranes cover several body regions and can be favourably used to target local disorders in order to achieve high-level dosing to the action site, reducing at the same time the systemic dose and minimizing the side effects. However, the presence of a gel mucus layer on mucosal surfaces represents a potential barrier for delivering drug molecules to the underlying epithelium (Lai et al., 2009). The diffusion through the mucus gel layer is even more challenging for molecules characterized by high hydrophilicity and molecular weight such as protein and peptide drugs (Thwala et al., 2017). In fact, the mucus is a three-dimensional network constantly renewed, consisting of negatively charged glycoproteins, called mucins and characterized by cysteine-rich subunits connected by disulfide bonds. Moreover, sulphate groups and sialic acid (pKa = 2.6) situated on the glycoprotein molecules result in mucin behaving as an anionic polyelectrolyte at neutral pH (Capra et al., 2007).

Nanoparticles (NPs) represent a valid option for peptide drug encapsulation and several formulation strategies based on polymeric nanocarriers have been developed for a more efficient mucosal delivery (Patel et al., 2014; Pawar et al., 2014). Particularly, it is possible to take advantage of two opposite properties showed by polymeric nanoparticulate systems, namely mucoadhesion and mucopenetration (Netsomboon and Bernkop-Schnürch, 2016).

Mucoadhesive polymeric NPs are able to adhere to the mucus gel layer, thus improving the retention time of the incorporated drug and promoting a site-specific delivery (Sosnik and Sarmento, 2014). Several mechanisms contribute to this adhesion, including physical entanglement of the polymeric chains, dehydration, electrostatic interaction, covalent bonds, and multiple low-affinity bonds, such as hydrogen bonds and Van der Waals forces (Andrews et al., 2009). Among explored polymers, chitosan (CH) is gaining increasing importance due to its well-known mucoadhesion ability. CH adheres to mucus mainly by means of ionic interactions between its amino groups and the sialic acid and sulphonic acid of glycoproteins (Bravo-Osuna et al., 2007; Sogias 2008). Cationic CH is also used to prepare cross-linked NPs, taking advantage of its ability to react with multivalent anions or anionic polymers (Berger et al., 2004a, 2004b). Hejjaji and colleagues evaluated the interaction between mucin and NPs with CH:sodium tripolyphosphate (TPP) ratios from 3:1 to 7:1 (Hejjaji et al., 2018). The results suggested that a minimum CH:TPP ratio of 4:1 is required to produce stable NPs with a great mucin binding efficiency. As regards polyelectrolyte complexes, CH-dextran sulfate NPs showed prolonged precorneal residence time (>4 h) following ocular administration as a result of the strong interaction between the positively charged NPs and the negatively charged mucus layer (Chaiyasan et al., 2017).

Mucopenetrating NPs show a high spreading ability over the mucosa and can penetrate deeper mucus regions, eventually reaching the underlying epithelium (Dünnhaupt et al., 2015). An improved penetration can be obtained by means of particles able to limit their interactions with mucus, namely particles exhibiting a high density of positive and negative charges, particles presenting a slippery surface and self-nanoemulsifying-drug-delivery-systems. Moreover, another interesting approach exploits the employment of particles able to interact with the mucus making it leakier, namely systems functionalized with disulfide

bridges breaking agents and with proteolytic enzymes (Dünnhaupt et al., 2015). Pereira de Sousa and colleagues developed highly densely charged surface NPs by combining CH with chondroitin exhibiting a 3-fold higher diffusion ability in intestinal mucus as compared to the reference 50/50 dl-lactide/glycolide copolymer NPs (Pereira de Sousa et al., 2015).

To the best of our knowledge, however, up to now a comparative study of the mucoadhesive and mucopenetrating properties of NPs obtained by cross-linking of the same cationic polymer with multivalent anions and anionic polymers has not been carried out. In the present study, we developed ionically crosslinked CH NPs with sodium carboxymethylcellulose (CMC), sodium alginate (ALG), sodium tripolyphosphate (TPP) and phytic acid (PA) that, *in virtue* of their mucoadhesive and mucopenetrating properties, could increase the peptide drug efficacy in the treatment of local intestinal diseases. Vancomycin (VM), a branched tricyclic glycosylated peptide antibiotic, was chosen as a model drug (Levine, 2006). Currently, it is administred by oral route when a local intestinal indication is envisaged, such as in patients with pseudomembranous enterocolitis, a disorder primarily caused by *Clostridium difficile* (Czepiel et al., 2019) and occasionally by *Staphylococcus aureus* (Gravet et al., 1999). VM is the drug of choice for the treatment of this disease because of its effectiveness against both of these Gram-positive pathogens and its poor absorption from the gastrointestinal tract (Dinu et al., 2020). Briefly, the main steps of this study were: (a) to prepare polymeric NPs via ionic interactions between CH and oppositely charged crosslinkers; (b) to characterize NPs in terms of size, polydispersity index, zeta-potential, morphology and drug encapsulation efficiency; (c) to investigate NP mucoadhesive ability and mucus permeating properties; (d) to confirm that VM being incorporated in NPs maintains its antimicrobial activity against Gram-positive bacterial species.

2. Materials and methods

2.1. Materials

The following chemicals were obtained from commercial sources and used as received. Chitosan 85/5 (CH; MW 10-50 kDa, deacetylation degree 82.6% - 87.5%) was purchased from Heppe medical chitosan GmbH (Saale, Germany). Sodium carboxymethylcellulose (CMC; MW 250 kDa, substitution degree 0.789) was purchased from A.C.E.F. (Piacenza, Italy). Sodium alginate (ALG; MW 140 kDa) was obtained from Carlo Erba (Milan, Italy). Vancomycin was kindly delivered from Hikma Italia (VM; Pavia, Italy). Penta-sodiumtripolyphosphate (TPP; MW 368 Da), phytic acid (PA; MW 660 Da), mucin from porcine stomach (type II, bound sialic acid ~1%) and all other salts and solvents at analytical grade were obtained from Sigma-Aldrich (Milan, Italy). Lumogen red 305 was purchased from Kremer Pigmente GmbH & Co. KG (Aichstetten, Germany). Nutrient Broth (NB) was supplied by Becton Dickinson and Company (Sparks, MD, USA). *Staphylococcus aureus* ATCC29213 and *Bacillus subtilis* ATCC31324 were delivered by ATCC (Manassas, VA, USA). Phosphate buffer at pH 7.4 (PBS) was composed of 2.38 g/L Na_2HPO_4 ×12 H_2O, 0.19 g/L KH_2PO_4 and 8.00 g/L NaCl. For HPLC method a phosphate buffer was prepared with 9.15 g/L Na_2HPO_4 x $12H_2O$ and adjusted at pH 7.0 with phosphoric acid.

2.2. Nanoparticle preparation

Nanoparticles (NPs) were prepared by ionic gelation method, through complexation of CH with different crosslinkers (CMC, ALG, TPP or PA). CH was solubilized in acetic acid (0.5 % v/v) for 24 hours under stirring at 200 rpm. After CH dissolution, the pH was adjusted at 5.6 with NaOH 2.5 % w/v (pHmeter, MicroPH CRISON 2000, Carpi, Italy), thus obtaining a cationic phase with CH concentration of 0.67 mg/mL. The anionic phase was obtained by dissolving the crosslinker (CMC, ALG, TPP or PA) in water under stirring at 200 rpm for 30 minutes at concentrations ranging from 0.25 mg/mL to 2 mg/mL. NPs were formed by adding the anionic phase (0.5 mL) to the cationic phase (1.5 mL) and maintaining the suspension under stirring for 15 minutes. For the preparation of loaded NPs, VM was added to CH solution (VM concentration equal to 5 mg/mL) before the addition of the anionic phase. To evaluate mucopenetrating properties, a fluorescent molecule was included in VM loaded NPs by adding 100 µL of a Lumogen solution (dimethylformamide, 0.15 mg/mL) to the cationic phase.

The resulting NP suspensions were centrifuged (Microspin 12, Highspeed Mini-centrifuge, Biosan, Riga, Latvia) on a glycerol bed at 14,000 rpm for 60 minutes at 25°C. Supernatants were discharged and the NPs-based pellets were re-suspended in ultrapure water (18.2 MΩ cm, MilliQ apparatus by Millipore, Milford, MA, USA).

2.3 Physicochemical characterization and determination of yield

Particle size and polydispersity index (PDI) were measured at 25°C by photon correlation spectroscopy (PCS) using a Brookhaven 90-PLUS instrument (Brookhaven Instruments Corp., Holtsville, NY, USA) with an He-Ne laser beam at a wavelength of 532 nm (scattering angle of 90°). For measurements, NP suspensions were dispersed in ultrapure water with a dilution of 1:40 (v/v). Zeta-potential measurements were carried out at 25 °C on a Malvern Zetasizer 3000 HS instrument (Malvern Panalytical Ltd., Malvern, UK) after the same dilution.

For the calculation of process yield, the NP suspensions were centrifuged (14,000 rpm, 60 minutes, T = 25°C) and the supernatants were discarded. The pellets were dried at 50°C (heating oven FD series, Binder, Tuttlingen, Germania) until constant weight, and the actual solid weights were obtained. The yield of the process was calculated as follows:

%Yield = Actual solid weight x 100/ Theoretical solid weight

2.4 Fourier Transformed Infrared Spectroscopy (FT-IR)

FT-IR spectra of CH, CMC, ALG, TPP, PA and unloaded NPs were recorded with a Jasco FT-IR 4100 spectrophotometer (Jasco, Lecco, Italy) in order to study the interactions between CH and the different crosslinkers. NP suspensions, obtained as described in section 2.2, were frozen overnight at -20°C and subsequently freeze-dried at 0.01 atm and -45°C (Freeze Dryer ALPHA 1-2, Christ, Milan, Italy). The samples were prepared as compressed KBr disks (NPs/KBr 1:10 w/w).

2.5 Determination of encapsulation efficiency and drug loading

For the calculation of the drug encapsulation efficiency (EE %) and drug loading (DL %), loaded NP suspensions, obtained as described in section 2.2, were centrifuged and the supernatants were adequately diluted in the mobile phase used for VM determination by HPLC method (Bigucci et al., 2008). Briefly, the chromatographic system was composed of a Shimadzu (Milan, Italy) LC-10ATVP chromatographic pump and a Shimadzu SPD-10AVP UV-vis detector set at 229 nm. Separation was carried out on a Phenomenex (Torrance, CA, USA) Synergi Fusion-RP 80A (150 mm x 4.6 mm I.D., 5 mm) coupled to a Phenomenex (Torrance, CA, USA) Security Guard C18 guard cartridge (4 mm x 3.0 mm I.D., 5 mm). Manual injections of samples were performed using a Rheodyne 7125 injector with a 20 µL sample loop. The mobile phase was a mixture of acetonitrile and sodium phosphate buffer at pH 7.0 (10:90 v/v) and the flow rate was 0.4 mL/min. Data processing was handled by means of a CromatoPlus computerized integration system (Shimadzu Italia, Milan, Italy). Calibration curve was obtained by dissolution of VM in the same media of the testing sample and their subsequent adequate dilutions in the mobile phase. Curve was plotted at concentration range of 0.005-0.1 mg/mL and a good linearity was found (R^2 = 0.9985).

The EE % and DL % were calculated using the following equations:

EE % = (Total amount of VM -Amount of non-entrapped VM) x 100/ Total amount of VM

DL % = (Total amount of VM -Amount of non-entrapped VM) x 100/ NP weight

2.6 Morphology

The morphology of NPs was investigated with atomic force microscopy (AFM). AFM imaging was performed in air in PeakForce Tapping®-mode on a Multimode 8 Nanoscope system (Bruker) using ScanAsyst Air probes (Bruker, Karlsruhe, Germany). An aliquot of NP suspension was layered on a disc of freshly cleaved mica and left to adsorb on the surface for about 10 min. The sample was then dehydrated under a gentle flow of nitrogen. The adsorbed NPs were then imaged in air in different locations on the dried sample. The apparent diameter was calculated employing the *Particle Analysis* tool of the software NanoScope Analsys (Bruker). A threshold height of 10 nm was applied to the flattened image, and the section area of the objects was used to estimate the diameter of the particles.

2.7 NP stability

NP stability was assessed by monitoring the size and the PDI over 60 days of storage at +4-8°C. At defined times (7, 15, 30 and 60 days), aliquots of fresh NP suspensions were diluted in water (1:40 v/v) and the change of NP size and PDI was measured using PCS as described in section 2.3.

2.8 Mucoadhesion properties

The mucoadhesive properties of unloaded NPs were evaluated by a method previously described by Yen and co-workers (Yin et al., 2006) with some modifications. NP suspension was mixed (1:1 v/v) with mucin dispersion (0.1 mg/mL), incubated at 37°C for 60 minutes and subsequently centrifuged at 10,000 rpm for 30

minutes. The remaining free mucin in the supernatant was determined at 261 nm by UV spectrophotometry (UV–Visible Spectrophotometer, Shimadzu Corporation, Australia) and related to the control (sample without NPs). The mucin binding efficiency of NPs was calculated using the following equation:

Mucin binding efficiency % = ($ABS_{control}$- ABS_{sample}) x 100/ $ABS_{control}$

An additional method based on turbidimetric measurements was employed in order to assess the mucoadhesive properties of unloaded and loaded NPs (Abruzzo et al., 2018). For this study, mucin was dispersed in water (0.08% w/v) for 6 hours. Then, mucin dispersion was centrifuged at 7500 rpm for 20 minutes to separate excess amount of mucin. Mucin dispersion and NP suspension were then mixed (1:3 v/v) and vortexed for 15 minutes. The turbidity of the sample was measured at 650 nm. The absorbance (ABS) of mucin dispersion itself and NP suspension without mucin were also measured as references. The increase % in turbidity at 650 nm with respect to NPs suspensions reflects NP interaction with the mucin and consequently the mucoadhesive characteristic of the sample, and was calculated as follows:

Turbidity increase % = ($ABS_{NPs+mucin}$- $ABS_{control}$) x 100/ ABS_{NPs}

2.9 Mucopenetrating properties

In order to predict the transport of NPs across the mucus barrier, a diffusion study through mucin was performed following a previously described technique with some modifications (Dunnhaupt et al., 2011). For this study, mucin was dispersed in water (5 mg/mL) at 25 °C for 24 hours and subsequently put in a silicon tube (4 cm length and 1 cm diameter), closed at one end, using a syringe without needle. Afterwards, the suspension (1 mL) of VM/Lumogen NPs was applied to the open end of the tube and then closed. All the tubes were kept under horizontal rotation at 50 rpm in an incubator (Certomat®Sartorius AG, Göttingen, Germany) at 37°C for 4 hours and then frozen at -20°C. Afterwards, the tubes were cut into slices of 3 mm length and each slice was incubated with 2 mL of dymethylformamide overnight at 25°C and protected from light in order to extract the encapsulated Lumogen. Samples were ultrasonicated for 1 hour and subsequently centrifuged for 2 minutes at 13,000 rpm to separate the mucin from the supernatant. The fluorescence intensity of the supernatant was determined in order to assess the depth of NP diffusion into the mucin (Fluorimeter FP8000, Jasco, Lecco, Italy; λ_{ex} 578 nm, λ_{em} 613 nm). Data were compared with the corresponding calibration curve elaborated in the same conditions.

2.10 *In vitro* drug release

For this study, NP suspensions (150 µL) were placed inside a becker containing 2 mL of PBS and stirred by using a magnetic stirrer at 200 rpm. At predetermined time intervals (30, 120, 240 minutes), aliquots of the sample were taken from the medium and centrifuged at 14,500 rpm for 15 minutes. The supernatants were filtered through a 0.22 µm pore size cellulose acetate filter (MF-Millipore Membrane, Tullagreen, Carrigtwohill, Co. Cork, Ireland) and analyzed through HPLC. VM release over time was determined as Mt/M0 (fractional amount), where Mt represents the amount of VM released at each time and M0 the total VM mass loaded into the NPs.

2.11 Antimicrobial activity

The antimicrobial activity of NPs towards *S. aureus* ATCC29213 and *B. subtilis* ATCC31324 was evaluated by broth microdilution following the EUCAST guidelines (EUCAST, 2020). Microorganisms were aerobically cultured on Nutrient agar plates at 37°C for 24 hours, and subsequently diluted in NB to obtain bacterial suspensions at final concentrations of 10^6 CFU/mL.

NP suspensions and VM solution, containing the same amount of drug, were diluted in sterile water in a two-fold sequence inside 96-well culture plates (Corning Inc., Pisa, Italy) in order to test VM concentrations ranging from 55 μg/mL to 0.03 μg/mL. Unloaded NPs were also tested at the same dilutions. The microbial suspension (50 μL) was then inoculated along with 50 μL of samples. Wells containing microbial suspension (50 μL) and sterile water (50 μL) served as growth control. Blank control, consisting only of growth medium, and sterility controls, containing formulations and sterile medium, were also included. Plates were aerobically incubated at 37°C for 24 hours. Afterwards, the minimal inhibiting concentration (MIC) was established by comparing the turbidity (OD_{600}) of samples with that of growth control by means of EnSpire Multimode Plate Reader (PerkinElmer Inc., Waltham, MA).

To determine a microbicidal effect, 20 μL of samples from wells exhibiting no growth were spotted onto Nutrient agar plates and incubated at 37 °C for further 48 h. MLC was defined as the minimal concentration that completely inhibited microbial viability.

2.12 Statistical analysis

All the experiments were performed in triplicate. The results were expressed as mean ± standard deviation (S.D.). For all the performed studies, Student's t-test was used to determine statistical significance. Differences were deemed significant for $p < 0.05$.

3. Results and discussion

3.1 NP preparation

NPs were prepared through the ionic gelation method, by exploiting the ability of CH to interact with the different crosslinkers thus providing colloidal particles. Specifically, at the pH of the final suspension (5.6), ionic interactions are possible due to the presence of positively charged amino groups of CH (pKa= 6.0-6.5; Sorlier et al., 2001) and the negatively charges of carboxylic groups of CMC (pKa= 4.3; Bigucci et al., 2015) and ALG (pKa= 3.14; Shi et al., 2006) and phosphate groups of TPP (pKa_3 = 2.8, pKa_4 = 6.5 and pKa_5 = 9.2; Cai and Lapitsky, 2017) and PA ($pKa_{1\text{-}6}$ 1.5, $pKa_{7\text{-}9}$= 5.7 -7.6, $pKa_{10\text{-}12}$ > 10; Costello et al., 1976). The method for NP preparation was simple, fast and mild as water-soluble molecules were employed and no organic solvents were included. However, it is well-known that NP formation is influenced by several factors, such as the polymer and crosslinker concentrations as well as their molecular weight and ionization degree (Abruzzo et al., 2019; Abruzzo et al, 2016; Cerchiara et al., 2015). Therefore, preliminary experiments were performed through visual observation of the suspensions in order to optimize

CH/crosslinkers weight ratios for NP preparation and isolation. As reported in Table 1, anionic phases containing different concentrations of crosslinker were prepared and added to the cationic phase. The appearance of the final system changed from a clear solution to a suspension with a high turbidity or a precipitate, depending on the crosslinker and its concentration. Specifically, a high turbidity was obtained when TPP or PA were employed, probably due to the high crosslinking ability of low molecular weight crosslinkers; while in the presence of crosslinkers with a higher molecular weight (CMC and ALG), interactions were hampered and a low turbidity was observed. Moreover, when crosslinker concentrations were too low or high, a clear solution (low crosslinking degree) or a very high turbidity (high crosslinking degree) were observed, indicating the presence of a low amount of NPs or precipitate, respectively. These data were in agreement with previous results reported by Hashad and colleagues (Hashad et al., 2016). In fact, a high dilution of the formulation medium can generate extensive spatial distance between polymer chains and crosslinkers, that consequently limits possible crosslinking. On the other hand, the excessive concentration can strongly reduce spatial distance thus implementing the crosslinking.

With the focus on obtaining a final suspension containing an adequate amount of nanometric particles, suspensions with high, medium and low turbidity were selected and further studied for the evaluation of the particle size.

3.2 Physicochemical characterization and determination of yield

The particle size and PDI are important parameters to control the NP stability over the time. Moreover, NP size and PDI significantly influence their functional characteristics, e.g. mucoadhesive/mucopenetrating properties, drug release and consequently biological performance (Lazaridou et al., 2020; Maffettone et al., 2010). Figure 1 reports the change of unloaded NP size as a function of crosslinker concentrations.

Generally, in the presence of increasing amount of crosslinker, an increase in size of unloaded NPs was observed. This result could be attributed to the higher content of negative charges able to promote CH crosslinking, in agreement with previous results (Lazaridou et al., 2020; Abruzzo et al., 2019; Abruzzo et al., 2016; Singh and Shinde, 2011). Moreover, for all the anionic phases, the concentration of crosslinker able to provide NPs was equal to 0.5 mg/mL and for this reason, this concentration was selected for further evaluations and to formulate VM loaded NPs.

At this concentration, the size of unloaded CH/CMC NPs were lower than unloaded CH/ALG NPs (Table 2, $p < 0.05$). This result could be related to the presence at pH 5.6 of a lower amount of charges and ionization degree of CMC (pKa 4.3, substitution degree 0.789) with respect to ALG (pKa= 3.14, one carboxylic group per monomer). Additionally, PA, containing a higher content of charged groups, demonstrated a greater crosslinking ability with respect to TPP, and provided the formation of NPs with a greater size ($p < 0.05$). The same trend was observed for loaded NPs (Table 3). Moreover, loaded NPs showed a greater size with respect to the unloaded ones ($p < 0.05$), probably due to the entrapment of drug inside the nanocarriers structure, in agreement with previously published data (Cerchiara et al., 2017).

The PDI value reflects the NP size distribution and is useful to estimate the dimensional uniformity of a particle sample (Danaei et al., 2020). As it can be seen from Tables 2 and 3, all the NPs presented low PDI values (< 0.3), thus indicating the homogeneity of NP suspensions (Ciro et al., 2020; Zweers et al., 2003).

The measurement of zeta-potential represents a crucial aspect considering that the superficial charge of NPs could impact on their stability and mucoadhesive/mucopenetrating properties. In fact, as reported in literature, higher values of zeta-potential favor higher electrostatic repulsion among the NPs and, consequently, a greater stability (Dong and Feng, 2004). Furthermore, considering the negative net charge of mucus layer, it has been reported that positively charged NPs interact with the mucus and get trapped, whereas slightly negatively charged or neutral NPs could more easily penetrate the mucus (Lai et al., 2009; Pereira de Sousa et al., 2015). As shown in Table 2 and 3, all the prepared formulations were characterized by positive zeta-potential, thus indicating the presence of the positively charged CH chains on the NP surface (Abruzzo et al., 2019). Among all the formulations, CH/CMC and CH/TPP NPs showed the lowest and highest value of zeta-potential, respectively, confirming a different ability of CMC and TPP to crosslink CH chains. Moreover, an increase in zeta-potential values was observed in the presence of VM ($p < 0.05$). In fact, as reported in previous works (Dinu et al., 2020; Takacs-Novak et al., 1993), at pH < 8.5 VM possess positive charges, able to interact with the different crosslinkers and to increase the net superficial charge of NPs.

Another crucial and challenging aspect in the design and formulation of nanoparticulate systems is to obtain a high yield (Hashad et al., 2016). Among all the formulations, CH/ALG NPs showed the lowest yield values ($p < 0.05$), while no significant differences were observed between yield values of the other NPs (medium values equal to 39.3% and 48.1% for unloaded and loaded NPs, respectively). Furthermore, for every type of crosslinker, loaded NPs revealed higher yield values with respect to the unloaded ones ($p > 0.05$), probably due to VM ability to interact with the different crosslinkers.

3.3 Fourier Transformed Infrared Spectroscopy (FT-IR)

In order to confirm the interaction between CH and the different crosslinkers, FT-IR spectra of the raw materials and unloaded NPs were obtained. Figure 2 shows the overlapped FT-IR spectra of CH (green trace), crosslinkers (blue traces) and unloaded CH/CMC, CH/ALG, CH/TPP and CH/PA NPs (red traces). The FT-IR spectrum of CH (green trace in Fig. 2 a-d) shows characteristic peaks at 1561 cm^{-1}, 1638 cm^{-1} and 3428 cm^{-1}, due to the presence of $-NH_2$, CH_3-C=O and -OH groups, respectively (Cerchiara et al., 2003). Regarding FT-IR spectra of CMC and ALG (blue traces in Fig. 2a and 2b), the large peak within the range of 3100-3600 cm^{-1} was the axial deformation of -OH, while at around 2900 cm^{-1} appeared the axial deformation of C-H (symmetrical and asymmetrical stretching of CH_3 or even groups of CH_2). Moreover, CMC showed peaks at 1617 cm^{-1} and 1421 cm^{-1} attributed to the asymmetrical and symmetrical stretching of -COO groups (Bigucci et al., 2015). In the FT-IR of ALG the typical band relative to the vibration of C=O group appeared at 1610 cm^{-1} (Abruzzo et al., 2013). The spectra of TPP and PA (blue traces in Fig. 2c and 2d) showed an absorption peak at 1211 cm^{-1} which indicated P=O stretching (Dudhani and Kosaraju, 2010). In the IR

spectra of NPs (red traces in Fig. 2a-d) the -NH_2 peak of CH shifted from 1561 cm^{-1} to 1580 cm^{-1}, thus confirming that amino groups were involved in the cross-linking by carboxylic or phosphate groups (Bigucci et al., 2015; Abruzzo et al., 2013; Dudhani and Kosaraju, 2010; Mohy Eldin et al., 2015).

3.4 Determination of encapsulation efficiency and drug loading

Encapsulation efficiency (EE%) and drug loading (DL%) represent critical parameters in the evaluation of the potential of a nanocarrier. The preparation of VM-loaded NPs could be challenging due to its high aqueous solubility that limits its loading into NPs. As it can be seen from Table 3, no significant difference in EE % and DL % was observed ($p > 0.05$) among the developed NPs. The mean EE % and DL % values were around 35 % and 49 %, respectively. These findings are in agreement with previous works, concerning the encapsulation of hydrophilic drugs inside CH NPs. Lazaridou and co-workers obtained EE % values lower than 50 % for CH/TPP NPs containing deferoxamine mesylate, attributing this result to the high water solubility of the drug (Lazaridou et al., 2020). Similar results were also obtained in our previous works (Cerchiara et al., 2015; Cerchiara et al., 2017) in which CH/TPP NPs loaded with VM were prepared using different CH/TPP molar ratios. Moreover, our results fit with data published by Goycoolea and colleagues, who prepared CH/TPP/ALG NPs for insulin transmucosal delivery, obtaining insulin loading efficiencies around 50 % (Goycoolea et al., 2009).

3.5 Morphology

AFM analysis was performed in order to gather information about the morphology of NPs and their size dispersion. The apparent diameter ranged from about 100 to 200 nm for bigger particles, although smaller nanoparticles were also detected, with apparent diameter of about 50 nm (Figure 3). In general CH/CMC, CH/TPP and CH/PA NPs were monodispersed, with round shape, and no significant differences were detected in presence of VM. CH/PA NPs were found to be more prone to form aggregates. This could be related to the larger size and higher turbidity observed compared to the other NPs. CH/ALG NPs showed a more complex morphology, as discrete individual particles with heterogeneous shape. As NPs were analyzed on partially dehydrated and surface-adsorbed specimens, it is possible that a certain degree of shrinking occurred, together with some inevitable shape adaptation on the substrate surface, coherent with what previously reported for CH NPs especially in comparison with PCS data (Abruzzo et al., 2016). Differences in the morphology and the degree of shrinkage may be dependent on the different properties of the crosslinkers, affecting the interaction between NPs and the surface in such conditions.

3.6 NP stability

The stability of NPs is one of the most critical issues, as their general tendency is to aggregate upon storage (Garcia-Fuentes et al., 2003). Figure 4 shows the change of size of unloaded and loaded NPs, monitored over a period of 60 days at +4-8°C.

As it can be seen, for unloaded CH/TPP and CH/PA NPs only a slight increase in size was observed after 60 days of storage ($p < 0.05$): these NPs reached dimensions equal to 232.1 ± 21.3 nm (from 170.7 ± 9.1 nm; % increase of 36%) and 328.6 ± 34.1 nm (from 256.7 ± 18.0 nm; % increase of 28%), respectively. Moreover, no significant difference in size was obtained for loaded CH/TPP NPs (from 221.8 ± 5.3 nm to 230.0 ± 5.7 nm) and CH/PA NPs (from 285.0 ± 7.1 nm to 294.1 ± 4.9 nm). Additionally, for these formulations, no relevant changes with respect to PDI was detected and the PDI values were maintained lower than 0.3 during all the storage period (data not shown). In general, the maintenance of size during the storage could be ascribed to the positive zeta-potential values that probably limited the aggregation and precipitation of the NPs. These results agree with previous findings reporting that high values of zeta-potential favor electrostatic repulsion among the particles and, consequently, their stability (Dong and Feng, 2004).

As regard NPs based on CH and polymeric crosslinkers, for unloaded CH/CMC NPs, a more evident increase in size was observed, reaching dimensions equal to 232.9 ± 11.1 nm (from 151.1 ± 12.9 nm; % increase of 54%); while a lower increase in size ($p< 0.05$) was obtained for the loaded ones (from 194.7 ± 5.6 nm to 224.3 ± 1.9 nm; % increase of 14%). However, PDI values were maintained lower than 0.3 for all the tested period (data not shown). Additionally, unloaded and loaded CH/ALG NPs showed a low stability over the time, reaching a final diameter equal to 846.9 ± 73.9 nm (from 305.0 ± 10.5 nm; % increase of 177%) and 543.0 ± 7.4 nm (from 350.1 ± 14.5 nm; % increase of 54%), respectively. This result could be attributed to the hydration ability of polymers, favored by the presence of hydrophilic and negatively charged carboxylic groups able to facilitate the entry of water into the nanostructure and consequently lead to the increase in size. Particularly, as previously reported, ALG is characterized by a higher amount of charges and ionization degree with respect to CMC, and this could explain the greater increase in size of CH/ALG NPs with respect to CH/CMC NPs ($p < 0.05$). Our findings are also in agreement with results reported by Choukaife and co-workers, who observed that ALG based NPs were generally characterized by high swelling due to their high hydrophilicity that caused low stability (Choukaife et al., 2020). In conclusion, the employment of different crosslinkers allowed to obtain NPs with different stability over the time. Specifically, among all the formulations, CH/TPP, CH/PA and CH/CMC NPs showed a good stability over the time, with a minimal or no increase in size during the storage period and could represent potential nanocarriers useful for drug delivery.

3.7 Mucoadhesion properties

Mucin is the major component of the mucus coating the cell lining of the digestive tract (Cone, 2009). The evaluation of interaction between NPs and mucin can be useful in order to assess their mucoadhesive behavior. Specifically, mucoadhesion properties were investigated by employing two different methods. For unloaded NPs, mucoadhesive studies were performed by measuring the amount of unbound mucin after the contact with NPs through UV spectrophotometry (261 nm). Only unloaded NPs were tested due to the VM absorption at the selected wavelength. Data reported in Table 4 (mucin binding efficiency %) demonstrated that CH/TPP NPs possessed the best mucoadhesive capacity among all the particles, while CH/CMC NPs the

lowest ability to bind mucin. These results could be related to the zeta-potential values. In fact, a more positive superficial charge led to higher mucoadhesive property, as a consequence of the interaction between the positive charges of CH and the negatively charged groups of mucus (sulfonic acid and sialic acid residues) (Hejjaji et al., 2018; Abruzzo et al., 2017; Cerchiara et al., 2016).

Additionally, mucoadhesion ability was investigated by measuring the turbidity at 650 nm of unloaded and loaded NPs in the presence or not of mucin, and results (Table 4) are expressed as turbidity increase (%). Indeed, the ABS measured for suspensions of NPs was due to scattering; in the presence of mucin, an increase of the % ABS (percentage increase of the sample ABS in the presence of mucin with respect to the same samples without mucin) was observed. In general, NPs with the highest positive zeta-potential, e.g. CH/TPP NPs, showed the greatest mucoadhesive ability, confirming the same trend observed with the previous method. However, no significant difference was observed between the other NPs ($p > 0.05$). Therefore, these data suggest that the selection of a suitable crosslinker allowed to modulate the mucoadhesive properties of NPs. Specifically, the employment of TPP as crosslinker led to the formation of NPs with high mucoadhesive ability, that could probably prolong the drug residence time at the mucosal site. However, a high interaction of NPs with the mucin could also determine their entrapment inside the mucus structure and limit their diffusion, thus hindering the reaching of the underlying epithelium. Instead, CH/CMC NPs, characterized by a lower ability to interact with the mucin, could get trapped to a lesser extend inside the mucus and easily penetrate through it.

3.8 Mucopenetrating properties

The rotating tube assay was employed to evaluate the penetration capacity of NPs through the mucus exploiting their ability to traverse a tube containing the mucin suspension under the exposure of rotation. To detect NPs during the diffusion study, VM loaded NPs containing a fluorescent molecule, Lumogen red, were prepared. No significant difference was observed between size, PDI and zeta-potential values of VM/Lumogen loaded NPs and VM loaded NPs (data not shown).

As depicted in Figure 5, CH/TPP and CH/ALG NPs remained primarily close to the starting point of the tubes (slices 2-6), whereas CH/CMC and CH/PA NPs diffused through the tube reaching the middle/last sections of mucin suspension (slices 8-11). This result could be attributed to the zeta-potential values of NPs. In fact, CH/TPP NPs, showing the more positive surface charge, were mainly able to interact with mucin and their diffusion is limited. On the other side, CH/CMC and CH/PA NPs, bearing a lower zeta-potential value, penetrated the mucus to a comparatively higher extent. Moreover, despite the zeta-potential value of CH/ALG NPs, a limited diffusion of these NPs was observed. This behavior could be related to the larger size of CH/ALG NPs with respect to the other NPs, which reduced their mobility as consequence of the physical entrapment. As previously reported, to penetrate mucus, nanocarriers must be small enough to avoid steric obstruction inside the dense porous structure of mucin fibers, cross-linked by hydrophobic interactions and disulfides links (Lai et al., 2009). Furthermore, our result is in agreement with data published by Norris and Sinko who studied the diffusion of particles with different size in reconstituted porcine gastric mucin gel,

and observed a sharp decrease in penetration ability when particle sizes reach 300 nm (Norris and Sinko, 1997). Data obtained with this test permitted to predict how the different crosslinkers impact on the NP ability to penetrate through the mucus. Interestingly, CH/CMC and CH/PA NPs were able to diffuse through the mucin, while the employment of TPP as crosslinker allowed to obtain NPs with a limited penetration ability, confirming the conclusion of the previous section. The development of nanocarriers possessing mucopenetrating properties represents an interesting approach to overcome the mucus layer, especially for the mucosal delivery of some peptide drugs, such as VM. In fact, it has been established that VM can form numerous hydrogen and ionic bonds with mucus glycoproteins and negatively charged residues, respectively, thanks to of its glycosidic structure and cationic net charge (Bernkop-Schnürch, 2018). Consequently, its permeation through the mucus and the consequent reaching of the underlying epithelium still remain challenging. Therefore, mucopenetrating NPs, such as CH/CMC and CH/PA NPs, could represent potential carriers to overcome the problem of low mucus permeation of peptide drugs and specifically, to ensure VM mucosal delivery.

3.9 *In vitro* drug release

The *in vitro* release rate of VM from the different NPs is depicted in Figure 6. No significant differences in the release behavior between the various formulations can be distinguished. Around 80% of VM was released within the first 30 min and nearly all of it was released within 120 min. This behavior is understood to be a consequence of the weak interaction of VM with NPs (Cerchiara et al., 2017).

3.10 Antimicrobial activity

Since VM action is limited to Gram-positive bacteria, *S. aureus* and *B. subtilis* were selected as model species in order to confirm the antibacterial activity of VM loaded inside NPs. Indeed, it is essential that the preparative process does not interfere with the biological activity of the formulated drug. As expected, free VM exerted strong antimicrobial activity against both *S. aureus* ATCC29213 and *B. subtilis* ATCC31324, as demonstrated by the low MIC values (0.86 μg/mL for *S. aureus* and 3.44 μg/mL for *B. subtilis*). Considering that VM acts by inhibiting the synthesis of the peptidoglycan that makes up the bacterial cell wall, it is not surprising that it resulted bactericidal at concentrations (MLD) above 1.74 μg/mL for *S. aureus* and 6.88 μg/mL for *B. subtilis*. Importantly, all loaded NPs exhibited the same MIC and MLD values as free VM, whilst unloaded NPs resulted inactive. These data show that NPs obtained with different crosslinkers were able to preserve the antimicrobial effects of VM. Moreover, the capacity of loaded NPs to completely abolish microbial viability after 24 hours of incubation is consistent with the complete release of drug occurring within 120 minutes (section 3.9).

Conclusion

Different NPs were prepared through ionic gelation method by exploiting the interaction between the positive charges of CH and the negative charges of different crosslinkers. NP sizes varied accordingly to the

molecular weight and ionization degree of crosslinker and all the developed NPs presented a positive zeta-potential and the ability to encapsulate VM. Moreover, CH/TPP NPs showed the best mucoadhesive properties, while CH/PA and CH/CMC NPs the best mucopenetrating ability. These results highlighted that the selection of a suitable crosslinker could allow to obtain different nanosystems with a prolonged residence time at the mucosal site or an improved diffusion across the mucus layer. Considering the limited diffusion of VM through the mucus gel layer, the employment of nanocarriers with mucopenetrating properties, such as CH/CMC and CH/PA NPs, could represent an interesting approach to improve its permeation through the mucus and consequently to favor the reaching of the underlying epithelium. Finally, all the developed NPs allowed a fast and complete drug release and ensured the maintenance of drug antimicrobial activity against Gram-positive bacterial species. Based on these results, this work gives a contribution for further design of mucoadhesive and mucopenetrating NPs for mucosal delivery of peptide drugs.

Conflict of interest

No conflicts of interest.

Acknowledgments

This work was supported by the Italian Ministry for University and Scientific Research. The authors would also like to thank Giulia Malavolti and Sofia Cavina for their valuable contribution.

References

Abruzzo, A., Bigucci, F., Cerchiara, T., Saladini, B., Gallucci, M.C., Cruciani, F., Vitali, B., Luppi, B., 2013. Chitosan/alginate complexes for vaginal delivery of chlorhexidine digluconate. Carbohydr. Polym. 91, 651-658.

Abruzzo, A., Zuccheri, G., Belluti, F., Provenzano, S., Verardi, L., Bigucci, F., Cerchiara, T., Luppi, B., Calonghi, N., 2016. Chitosan nanoparticles for lipophilic anticancerdrug delivery: development, characterization and in vitro studies on HT29 cancer cells. Colloids Surf. B: Biointerfaces 145, 362-372.

Abruzzo, A., Nicoletta, F.P., Dalena, F., Cerchiara, T., Luppi, B., Bigucci, F., 2017. Bilayered buccal films as child-appropriate dosage form for systemic administration of propranolol. Int. J. Pharm. 531, 257-265.

Abruzzo, A., Giordani, B., Parolin, C.,Vitali, B., Protti, M., Mercolini, L., Cappelletti, M., Fedi, S., Bigucci, F., Cerchiara, T., Luppi, B., 2018. Novel mixed vesicles containing lactobacilli biosurfactant for vaginal delivery of an anti-Candida agent. Eur. J. Pharm. Sci. 112, 95-101.

Abruzzo, A., Cerchiara, T., Bigucci, F., Zuccheri, G., Cavallari, C., Saladini, B., Luppi B., 2019. Cromolyn-crosslinked chitosan nanoparticles for the treatment of allergic rhinitis. Eur. J. Pharm. Sci. 131, 136-145.

Andrews, G.P., Laverty, T.P., Jones, D.S., 2009. Mucoadhesive polymeric platforms for controlled drug delivery. Eur. J. Pharm. Biopharm. 71, 505-518.

Berger, J., Reist, M., Mayer, J.M., Felt, O., Peppas, N.A., Gurny, R., 2004a. Structure and interactions in covalently and ionically crosslinked chitosan hydrogels for biomedical applications. Eur. J. Pharm. Biopharm. 57, 19-34.

Berger, J., Reist, M., Mayer, J.M., Felt, O., Gurny, R., 2004b. Structure and interactions in chitosan hydrogels formed by complexation or aggregation for biomedical applications. Eur. J.Pharm. Biopharm. 57, 35-52.

Bernkop-Schnürch, A., 2018. Strategies to overcome the polycation dilemma in drug delivery. Adv. Drug Deliv. Rev. 136-137, 62-72.

Bigucci, F., Luppi, B., Musenga, A., Cerchiara, T., Zecchi, V., 2008. Chitosan salts coated with stearic acid as colon-specific delivery systems for vancomycin. Drug Deliv. 15, 289-293.

Bigucci, F., Abruzzo, A., Vitali, B., Saladini, B., Cerchiara, T., Gallucci, M.T., Luppi, B., 2015. Vaginal inserts based on chitosan and carboxymethylcellulose complexes for local delivery of chlorhexidine: preparation, characterization and antimicrobial activity. Int. J. Pharm. 478, 456-463.

Bravo-Osuna, I., Vauthier, C., Farabollini, A., Palmieri, G.F., Ponchel, G., 2007. Mucoadhesion mechanism of chitosan and thiolated chitosan-poly(isobutyl cyanoacrylate) core-shell nanoparticles. Biomaterials 28, 2233-2243.

Cai, Y., Lapitsky, Y., 2017. Analysis of chitosan/tripolyphosphate micro- and nanogel yields is key to understanding their protein uptake performance. J. Colloid Interface Sci. 494, 242-254.

Capra, R., Baruzzi, A., Quinzani, L., Strumia, M., 2007. Rheological, dielectric and diffusion analysis of mucin/carbopol matrices used in amperometric biosensors. Sens. Actuators B Chem. 124, 466-476.

Cerchiara, T., Luppi, B., Bigucci, F., Petrachi, M., Orienti, I., Zecchi V., 2003. Controlled release of vancomycin from freeze-dried chitosan salts coated with fatty acids by spray-drying, J. Microencapsul. 20, 473-478.

Cerchiara, T., Abruzzo, A., di Cagno, M., Bigucci, F., Bauer-Brandl, A., Parolin, C., Vitali, B., Gallucci, M.C., Luppi, B., 2015. Chitosan based micro- and nanoparticles for colon targeted delivery of vancomycin prepared by alternative processing methods. Eur. J. Pharm. Biopharm. 92, 112-119.

Cerchiara, T., Abruzzo, A., Parolin, C., Vitali, B., Bigucci, F., Gallucci, M.C., Nicoletta, F.P., Luppi, B., 2016. Microparticles based on chitosan/carboxymethylcellulose polyelectrolyte complexes for colon delivery of vancomycin. Carbohydr. Polym. 143, 124-130.

Cerchiara, T., Abruzzo, A., Ñahui Palomino, R.A., Vitali, B., De Rose, R., Chidichimo, G., Ceseracciu, L., Athanassiou, A., Saladini, B., Dalena, F., Bigucci, F., Luppi, B., 2017. Spanish Broom (Spartium junceum L.) fibers impregnated with vancomycin- loaded chitosan nanoparticles as new antibacterial wound dressing: Preparation, characterization and antibacterial activity. Eur. J. Pharm. Sci. 99, 105-112.

Chaiyasan, W., Praputbut, S., Kompella, U.B., Srinivas, S.P., Tiyaboonchai, W., 2017. Penetration of mucoadhesive chitosan-dextran sulfate nanoparticles into the porcine cornea. Colloids Surf. B Biointerfaces 149, 288-296.

Choukaife, H., Doolaanea, A.A., Alfatama, M., 2020. Alginate nanoformulation: Influence of process and selected variables. Pharmaceuticals (Basel) 13, 335-368.

Ciro, Y., Rojas, J., Alhajj, M.J., Carabali, G.A., Salamanca, C.H., 2020. Production and characterization of chitosan-polyanion nanoparticles by polyelectrolyte complexation assisted by high-intensity sonication for the modified release of methotrexate. Pharmaceuticals (Basel) 13, 11-24.

Cone, R.A. 2009. Barrier properties of mucus. Adv. Drug Deliv. Rev. 61, 75-85.

Costello, A.J.R., Glonek, T., Myers, T.C., 1976. Phosphorus-31 nuclear magnetic resonance – pH titration of hexaphosphate (phytic acid). Carbohydr. Res. 46, 156-171.

Czepiel, J., Dróżdż, M., Pituch, H., Kuijper E.J., Perucki, W., Mielimonka, A., Goldman, S., Wultańska, D., Garlicki, A., Biesiada, G., 2019. Clostridium difficile infection: review. Eur. J. Clin. Microbiol. Infect. Dis. 38, 1211-1221.

Danaei, M., Dehghankhold, M., Ataei, S., Hasanzadeh Davarani, F., Javanmard, R., Dokhani, A., Khorasani, S., Mozafari, M.R., 2018. Impact of particle size and polydispersity index on the clinical applications of Lipidic nanocarrier systems. Pharmaceutics 10, 57-73.

Dinu, V., Lu, Y., Weston, N., Lithgo, R., Coupe, H., Channell, G., Adams, G.G., Torcello Gómez, A., Sabater, C., Mackie, A., Parmenter, C., Fisk, I., Phillips-Jones, M.K., Harding, S.E., 2020.The antibiotic vancomycin induces complexation and aggregation of gastrointestinal and submaxillary mucins. Sci. Rep. 10, 960-971.

Dong, Y.; Feng, S.S., 2004. Methoxy poly(ethylene glycol)-poly(lactide) (MPEG-PLA) nanoparticles for controlled delivery of anticancer drugs. Biomaterials 25, 2843-2849.

Dudhani, A.R., Kosaraju, S.L., 2010. Bioadhesive chitosan nanoparticles: preparation and characterization. Carbohydr. Polym. 81, 243-251.

Dunnhaupt, S., Barthelmes, J., Hombach, J., Sakloetsakun, D., Arkhipova, V., Bernkop-Schnurch, A., 2011. Distribution of thiolated mucoadhesive nanoparticles on intestinal mucosa. Int. J. Pharm. 408, 191-199.

Dünnhaupt, S., Kammona, O., Waldner, C., Kiparissides, C., Bernkop-Schnürch, A., 2015. Nano-carrier systems: Strategies to overcome the mucus gel barrier. Eur. J. Pharm. Biopharm. 96, 447-453.

EUCAST-The European Committee on Antimicrobial Susceptibility Testing, 2020. EUCAST reading guide for broth microdilution.

https://www.eucast.org/fileadmin/src/media/PDFs/EUCAST_files/Disk_test_documents/2020_manuals/Reading_guide_BMD_v_2.0_2020.pdf.

Garcia-Fuentes, M., Torres, D., Alonso, M.J., 2003. Design of lipid nanoparticles for the oral delivery of hydrophilic macromolecules. Colloids Surf. B: Biointerf. 27, 159-168.

Goycoolea, F.M.; Lollo, G.; Remuñán-López, C.; Quaglia, F.; Alonso, M.J., 2009. Chitosan-alginate blended nanoparticles as carriers for the transmucosal delivery of macromolecules. Biomacromolecules 10, 1736-1743.

Gravet, A., Rondeau, M., Harf-Monteil, C., Grunenberger, F., Monteil, H., Scheftel, J.M., Prévost, G., 1999. Predominant Staphylococcus aureus isolated from antibiotic-associated diarrhea is clinically relevant and produces enterotoxin A and the biocomponent toxin LukE- LukK. J. Clin. Microbiol. 37, 4012-4019.

Hashad, R.A., Ishak, R.A., Fahmy, S., Mansour, S., Geneidi, A.S., 2016. Chitosan-tripolyphosphate nanoparticles: optimization of formulation parameters for improving process yield at a novel pH using artificial neural networks. Int. J. Biol. Macromol. 86, 50-58.

Hejjaji, E.MA., Smith, A.M., Morris, G.A., 2018. Evaluation of the mucoadhesive properties of chitosan nanoparticles prepared using different chitosan to tripolyphosphate (CS:TPP) ratios. Int. J. Biol. Macromol. 120, 1610-1617.

Lai, S.K., Wang, Y.Y., Hanes, J., 2009. Mucus-penetrating nanoparticles for drug and gene delivery to mucosal tissues. Adv. Drug Deliv. Rev. 61, 158-171.

Lazaridou, M., Christodoulou, E., Nerantzaki, M., Kostoglou, M., Lambropoulou, D.A., Katsarou, A., Pantopoulos, K., Bikiaris, D.N., 2020. Formulation and in-vitro characterization of chitosan-nanoparticles loaded with the iron chelator deferoxamine mesylate (DFO). Pharmaceutics 12, 238-254.

Levine, D.P., 2006. Vancomycin: a history. Clin Infect Dis. 42, S5-S12.

Maffettone, C., Chen, G., Drozdov, I., Ouzounis, C., Pantopoulos, K., 2010. Tumorigenic properties of iron regulatory protein 2 (IRP2) mediated by its specific 73-amino acids insert. PLoS ONE 5, e10163.

Mohy Eldin, M.S., Omer, A.M., Wassel, M.A., Tamer, T.M., Abd Elmonem, M.S., Ibrahim, S.A. 2015. Novel smart pH sensitive chitosan grafted alginate hydrogel microcapsule for oral protein delivery: II. Evaluation of the swelling behavior. Int. J. Pharm. Sci. 7, 320-326.

Netsomboon, K., Bernkop-Schnürch, A., 2016. Mucoadhesive vs. mucopenetrating particulate drug delivery. Eur. J. Pharm. Biopharm. 98, 76-89.

Norris, D.A., Sinko, P.J., 1997. Effect of size, surface charge, and hydrophobicity on the translocation of polystyrene microspheres through gastrointestinal mucin. J. Appl. Polym. Sci. 63, 1481-1492.

Patel, A., Patel, M., Yang, X., Mitra, A.K., 2014. Recent advances in protein and peptide drug delivery: A special emphasis on polymeric nanoparticles. Protein Pept. Lett. 21, 1102-1120.

Pawar, V.K., Meher, J.G., Singh, Y., Chaurasia, M., Surendar Reddy, B., Chourasia, M.K., 2014. Targeting of gastrointestinal tract for amended delivery of protein/peptide therapeutics: Strategies and industrial perspectives. J. Control. Release. 196, 168-183.

Pereira de Sousa, I., Steiner, C., Schmutzler, M., Wilcox, M.D., Veldhuis, G.J., Pearson, J.P., Huck, C.W., Salvenmoser, W., Bernkop-Schnürch, A., 2015. Mucus permeating carriers: formulation and characterization of highly densely charged nanoparticles. Eur. J. Pharm. Biopharm. 97, 273-279.

Shi, J., Alves, N.M., Mano, J.F., 2006. Drug release of pH/temperature-responsive calcium alginate/poly(N-isopropylacrylamide) semi-IPN beads. Macromol. Biosci. 6, 358-363.

Singh, K.H., Shinde, U.A., 2011. Chitosan nanoparticles for controlled delivery of brimonidine tartrate to the ocular membrane. Die Pharm. Int. J. Pharm. Sci. 66, 594-599.

Sogias, I.A., Williams, A.C., Khutoryanskiy, V.V., 2008. Why is chitosan mucoadhesive? Biomacromolecules 9, 1837-1842.

Sorlier, P., Denuzière, A., Viton, C., Domard, A., 2001. Relation between the degree of acetylation and the electrostatic properties of chitin and chitosan. Biomacromolecules 2, 765-772.

Sosnik, A., Sarmento, B., 2014. Progress in Polymer Science Mucoadhesive polymers in the design of nano-drug delivery systems for administration by non-parenteral routes: A review. Prog. Polym. Sci. 39, 2030-2075.

Takacs-Novak, K., Noszal, B., Tokes-Kovesdi, M., Szasz, G., 1993. Acid-base properties and proton-speciation of vancomycin. Int. J. Pharm. 89, 261-263.

Thwala, L.N., Préat, V., Csaba, N.S., 2017. Emerging delivery platforms for mucosal administration of biopharmaceuticals: a critical update on nasal, pulmonary and oral routes. Expert. Opin. Drug Deliv. 14, 23-36.

Yin, Y., Chen, D., Qiao, M., Lu, Z., Hu, H., 2006. Preparation and evaluation of lectin conjugated PLGA nanoparticles for oral delivery of thymopentin. J. Control. Release 116, 337-345.

Zweers, M.L.T., Grijpma, D.W., Engbers, G.H.M., Feijen, J., 2003. The preparation of monodisperse biodegradable polyester nanoparticles with a controlled size. J. Biomed. Mater. Res. B Appl. Biomater. 66, 559-566.

Figure 1. Unloaded NP size as function of different crosslinker concentrations.

Figure 2. FTIR spectrum of CH (green trace) superimposed with crosslinkers (blue trace) and NPs (red traces): (a) CH, CMC, CH/CMC NPs, (b) CH, ALG, CH/ALG NPs, (c) CH, TPP, CH/TPP NPs and (d) CH, PA, CH/PA NPs.

730 Figure 3. AFM images of a) CH/CMC, b) CH/PA, c) CH/TPP, d) CH/ALG. Heights in the images are color coded according to the attached look-up table on the right and the size bars below.

Figure 4. Variation of size of unloaded (a) and loaded (b) NPs during 60 days of storage at +4-8°C.

Figure 5. Diffusion studies of NPs trough porcine mucin.

Figure 6. VM release profiles from NPs in phosphate buffer at pH 7.4.

735

Table 1. Appearance of the final suspensions prepared with different concentrations of crosslinkers.

	Crosslinker concentration (mg/mL)				
Type of crosslinker	2	1	0.75	0.5	0.25
CMC	Precipitation	High turbidity	Medium turbidity	Medium turbidity	Clear solution
ALG	Precipitation	Precipitation	High turbidity	Medium turbidity	Low turbidity
TPP	Precipitation	Precipitation	Precipitation	Medium turbidity	Low turbidity
PA	Precipitation	Precipitation	Precipitation	Medium turbidity	Low turbidity

Table 2. Size (nm), polydispersity index (PDI), zeta-potential (mV) and yield % of the unloaded NPs.

Type of NPs	Size (nm)	PDI	Pot. ζ (mV)	Yield %
CH/CMC	151.1 ± 12.9	0.13 ± 0.02	+17.5 ± 0.4	43.5 ± 4.1
CH/ALG	305.0 ± 10.5	0.17 ± 0.06	+20.8 ± 0.9	32.2 ± 2.8
CH/TPP	170.7 ± 9.1	0.20 ± 0.03	+27.1 ± 1.6	38.2 ± 1.8
CH/PA	256.7 ± 18.0	0.21 ± 0.03	+23.7 ± 0.3	43.3 ± 3.7

Table 3. Size (nm), polydispersity index (PDI), zeta-potential (mV), yield %, encapsulation efficiency (EE %) and drug loading (DL %) of the loaded NPs.

Type of NPs	Size (nm)	PDI	Pot. ζ (mV)	Yield %	EE %	DL %
CH/CMC	194.7 ± 5.6	0.16 ± 0.02	+20.5 ± 0.6	53.0 ± 4.2	41.4 ± 6.1	52.0 ± 7.3
CH/ALG	350.1 ± 14.5	0.20 ± 0.01	+23.4 ± 1.0	42.0 ± 2.4	32.6 ± 7.3	51.8 ± 7.85
CH/TPP	221.8 ± 5.3	0.24 ± 0.02	+31.9 ± 1.7	47.1 ± 2.6	32.7 ± 7.9	46.4 ± 6.3
CH/PA	285.0 ± 7.1	0.21 ± 0.02	+28.0 ± 1.2	50.3 ± 3.0	33.8 ± 3.4	45.1 ± 5.6

Table 4. Mucoadhesive properties of unloaded and loaded NPs.

Type of NPs	Mucin binding efficiency %	Turbidity increase %	
		Unloaded NPs	Loaded NPs
CH/CMC	37.1 ± 1.4	173.7 ± 7.8	226.7 ± 22.7
CH/ALG	57.3 ± 2.1	206.7 ± 20.2	221.9 ± 31.7
CH/TPP	64.9 ± 2.1	328.4 ± 30.2	318.5 ± 31.9
CH/PA	58.8 ± 2.6	186.1 ± 20.9	218.5 ± 21.4

Figure 1

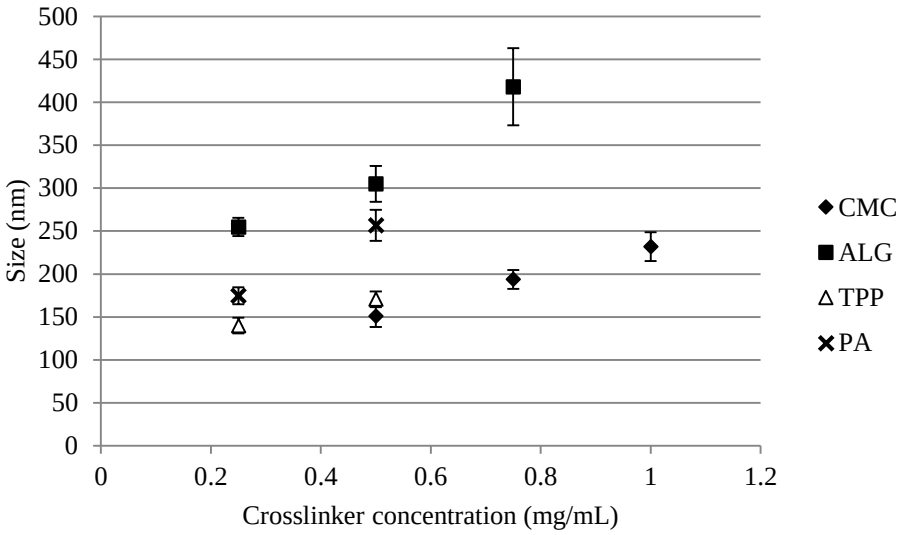
500
450
400
350
300
250
200
150
100
50
0
Size (nm)
0
0.2
0.4
0.6
0.8
1
1.2
Crosslinker concentration (mg/mL)
CMC
ALG
TPP
PA

Figure 2

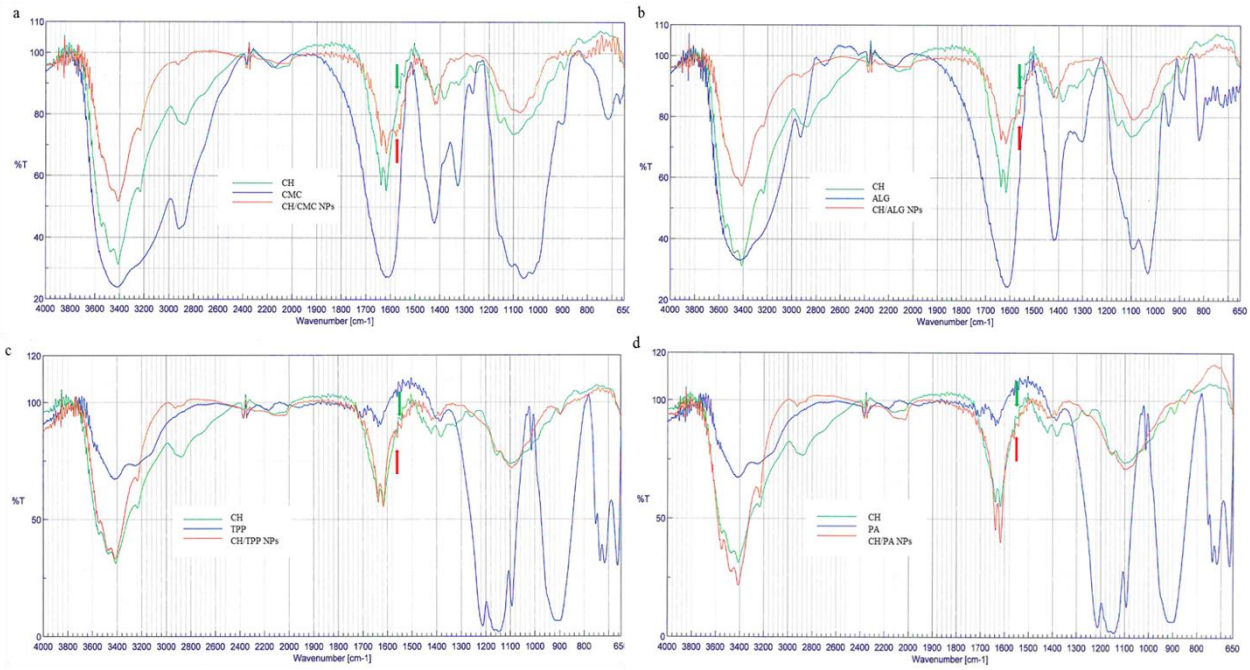
a
%T
CH
CMC
CH/CMC NPs
Wavenumber [cm-1]
b
%T
CH
ALG
CH/ALG NPs
Wavenumber [cm-1]
c
%T
CH
TPP
CH/TPP NPs
Wavenumber [cm-1]
d
%T
CH
PA
CH/PA NPs
Wavenumber [cm-1]

Figure 3

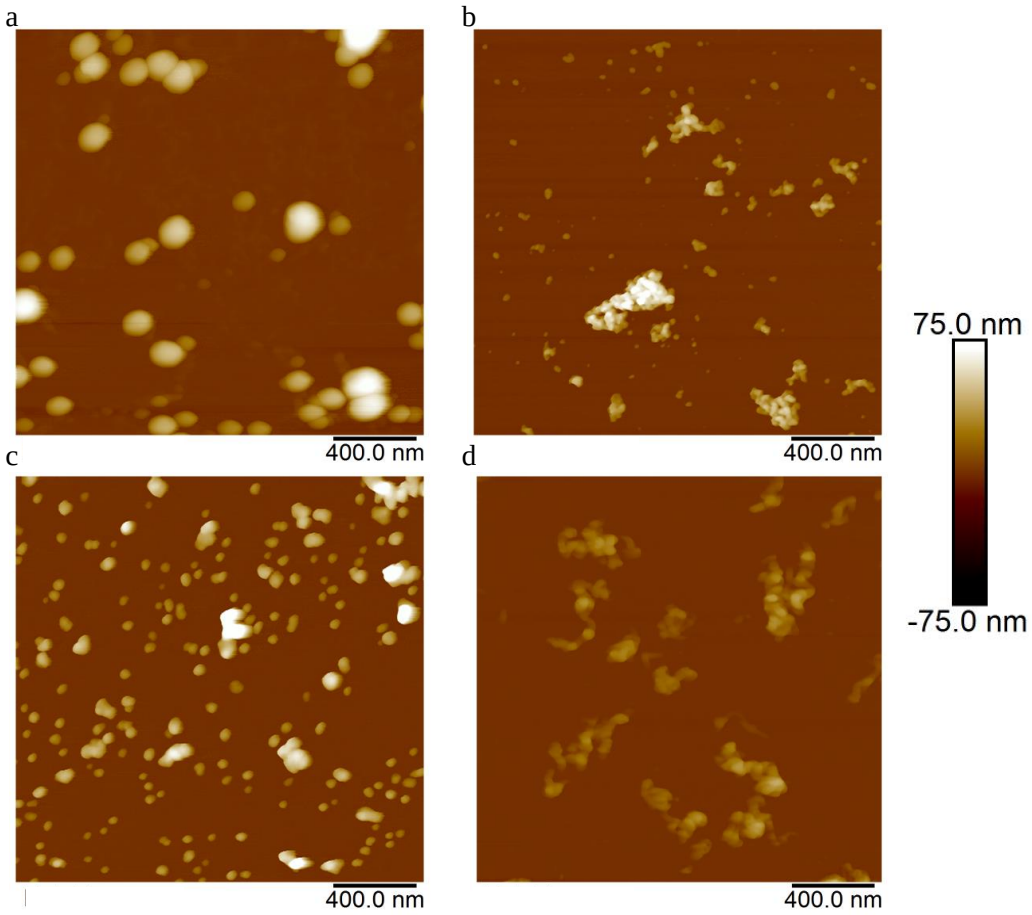

Figure 4

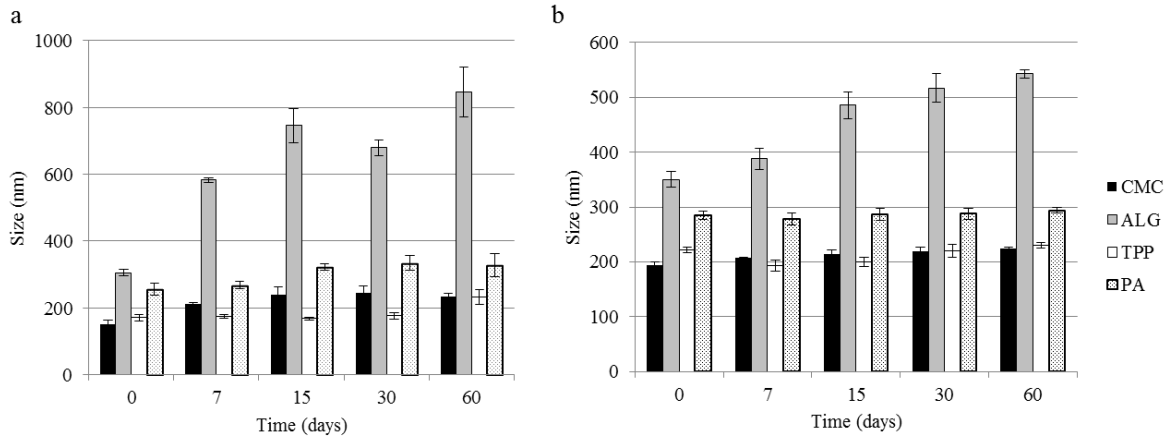
a
1000
800
600
400
200
0
Size (nm)
0
7
15
30
60
Time (days)
b
600
500
400
300
200
100
0
Size (nm)
0
7
15
30
60
Time (days)
CMC
ALG
TPP
PA

Figure 5

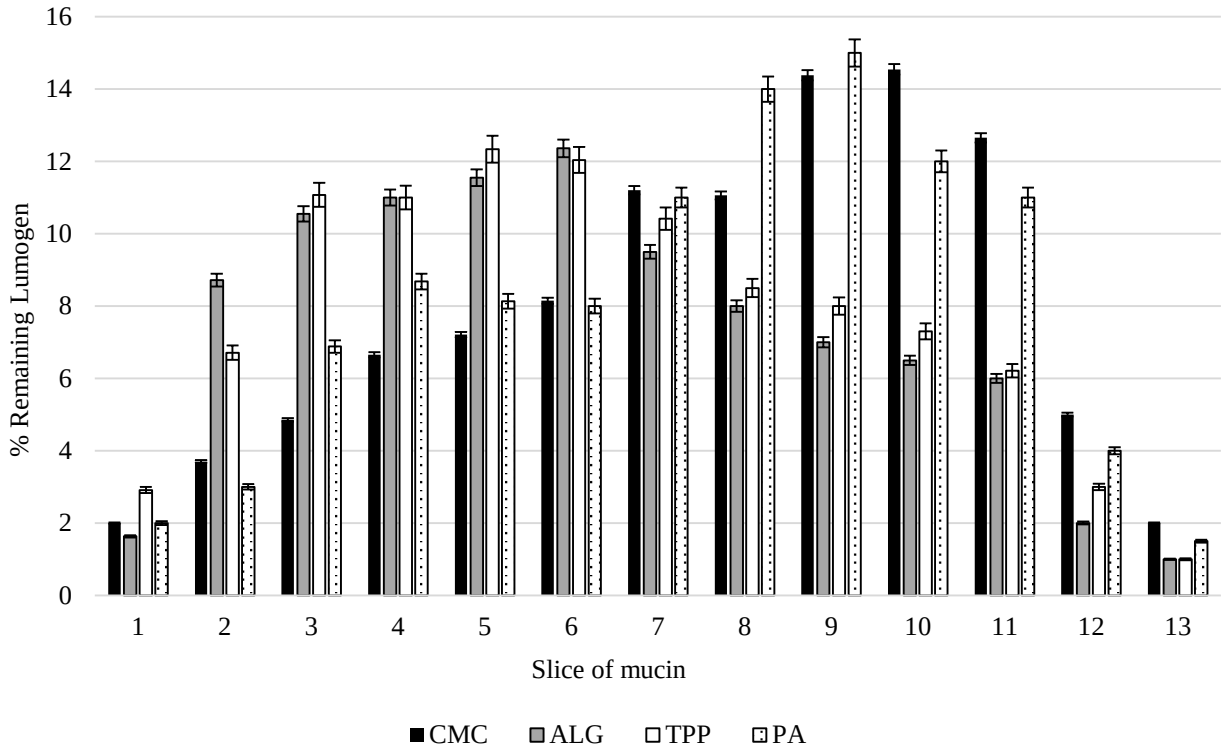
16
14
12
10
8
6
4
2
0
% Remaining Lumogen
1
2
3
4
5
6
7
8
9
10
11
12
13
Slice of mucin
CMC
ALG
TPP
PA

Figure 6

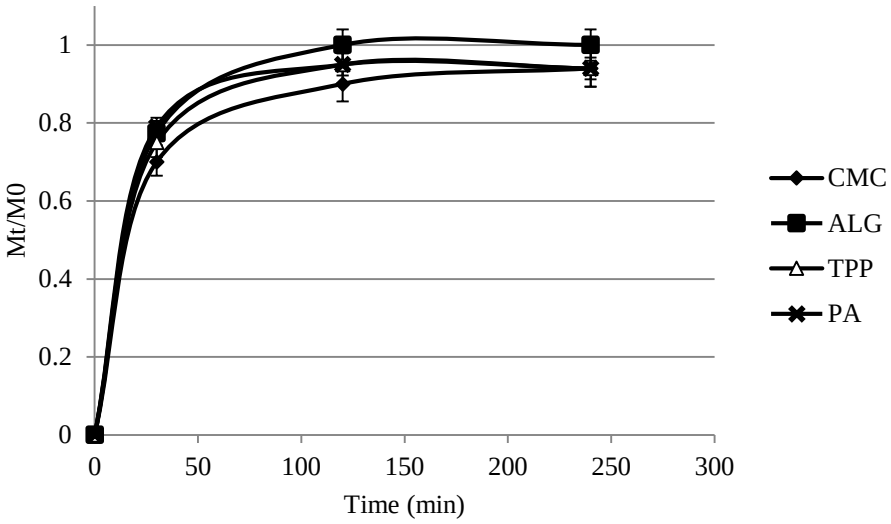
1
0.8
0.6
0.4
0.2
0
Mt/M0
0
50
100
150
200
250
300
Time (min)
CMC
ALG
TPP
PA

- Chitosan based nanoparticles (NPs) were prepared for vamcomycin (VM) delivery
- The selection of a suitable crosslinker allowed to modulate NP properties
- Chitosan/sodium tripolyphosphate NPs showed the best mucoadhesive ability
- Sodium carboxymethylcellulose and phytic acid provided the best mucopenetrating NPs
- NPs maintained VM antimicrobial activity against Gram-positive bacterial species

Declaration of interests

☒The authors declare that they have no known competing financial interests or personal relationships that could have appeared to influence the work reported in this paper.

☐The authors declare the following financial interests/personal relationships which may be considered as potential competing interests:

Credit Author Statement

Abruzzo Angela: Conceptualization, Methodology, Validation, Formal analysis, Investigation, Writing - Original Draft, Writing - Review & Editing. **Giordani Barbara:** Methodology, Validation, Formal analysis, Investigation, Writing - Original Draft. **Miti Andrea:** Methodology, Validation, Investigation, Writing - Original Draft. **Vitali Beatrice:** Methodology,Writing - Review & Editing. **Zuccheri Giampaolo:** Methodology,Writing - Review & Editing. **Cerchiara Teresa:** Writing - Review & Editing, **Luppi Barbara:** Writing - Review & Editing. **Bigucci Federica:** Conceptualization, Methodology, Writing - Original Draft, Writing - Review & Editing.